Formation, modulation and adaptive twinning of martensite in the $Au_7Cu_5Al_4$ shape memory system

M.B. Cortie[♣] and F.C. Levey

Mintek, Private Bag X3015, Randburg 2125, South Africa

Abstract

The $Au_7Cu_5Al_4$ β electron phase transforms displacively from an $L2_1$ parent to a nominally body-centred tetragonal martensite with *c*/a<1. The compound is of interest because it has the potential to serve as an 18 carat shape memory alloy in jewellery. Analysis of its X-ray diffraction spectra indicates that the martensite is modulated by a [110]/[$\bar{1}$10] transverse shear wave, showing that it belongs, strictly speaking, to the generic B19 structure type. The martensite is also twinned, and the probable twinning structure is explored. A $15R(9,\bar{6})$ stacking sequence is deduced, which for reasons of the $L2_1$ ordering inherited from the parent phase, must be doubled to produce a notional $30R(9,\bar{6},9,\bar{6})$ martensite that properly repeats. However, although the measured X-ray diffraction spectra can be substantially explained by the structures derived, the martensite probably also has additional, higher-order lattice modulations.

Keywords: martensite, shape memory alloy, X-ray diffraction, modulated structure, adaptive twining.

[♣] corresponding author, fax : +27-11-709-4480, email : mikec@mintek.co.za

1. Introduction

The reversible displacive transformation in certain 18 carat Au-Cu-Al alloys has inspired their application in jewellery, although details of the associated crystal structures and phase transformations were not originally known [1]. Later it was shown that the addition of 5.8 wt.% Al to face-centred cubic (Au,Cu) causes the structure at elevated temperatures to become body-centered cubic, with lattice parameter $a \approx 0.608$ nm and electron-to-atom ratio e/a of ≈ 1.48 [2]. This ternary β electron compound has the approximate stoichiometry $Au_7Cu_5Al_4$. It normally has strong B2 ordering, but ageing at between 100 and 200°C causes the development of a variable amount of $L2_1$ ordering. Only in this latter state does it undergo a martensitic transformation to a nominally body-centred tetragonal (bct) martensite with a 16 atom unit cell and lattice parameters of $a \approx 0.630$ nm and $c \approx 0.596$ nm [3,4]. The martensite has $c/a < 1$, which is an unusual situation since many martensites formed from body-centred cubic (bcc) parents are approximately close-packed with hexagonal, orthorhombic or monoclinic crystal structures, while most of the comparatively rare bct martensites that have been recorded have $c/a > 1$ [4]. The few example of bct martensites with $c/a < 1$ known to the authors are formed from La_2AgIn, Ni_2MnGa, AuMn and NiMn parent phases.

This paper addresses the structure of the $Au_7Cu_5Al_4$ martensite, and shows that its atoms are slightly displaced (‘modulated’ or ‘distorted’) from their nominal body-centred tetragonal lattice positions. The nature of the lattice modulation necessary to explain its X-ray diffraction (XRD) spectrum and fine-scale microstructure are explored.

2. Experimental

The procedures used to manufacture the alloy samples, characterise the phase transformations, measure the XRD spectra, and determine the lattice occupancies of the parent phase have been described elsewhere [2-4]. In brief, the samples were made by melting in a muffle furnace, and were then subjected to heat treatments of various kinds, with the results of the heat treatments being determined using optical metallography, acoustic emission and X-ray diffraction. The XRD spectra shown here were obtained with Mo k_α radiation.

Modulation of the lattice of the martensite was investigated with the aid of a computer program that ran within the Crystallographica♦ Pascal workspace. The program first constructed a unit cell with up to 250 atoms and the desired occupancies, which were presumed to be inherited from the parent phase, and then modulated it in terms of atomic position according to user dictates. The resulting structures were then used to calculate XRD spectra, and these were compared to the experimental spectra.

3. Mechanism of tetragonal martensite formation

3.1 The bcc to tetragonal transformation

It is known that the martensitic transformation of a bcc electron phase is driven by the increasing geometric instability of its lattice as the temperature decreases, and in particular by its tendency to achieve a more negative free energy by collapsing to a denser packing arrangement [4,5]. This is abetted in bcc parent lattices by their intrinsic geometric susceptibility to shear of the $\{110\}<1\bar{1}0>$-type [6,7]. This instability may also manifest in the form of a $<0\bar{1}1><011>$ phonon soft mode. In the most ideal case, a shear strain applied in the $[1\bar{1}0]$ direction along a (110) plane, accompanied by a

♦ Crystallographica is a product of Oxford Cryosystems, 3 Blenheim Office Park, Lower Road, Long Hanborough, Oxford OX8 8LN, UK.

lattice contraction in the perpendicular direction, will produce a fcc lattice from a bcc one [7]. Many of the copper-based martensite structures are readily explained as being the result of such shear; however, the actual structure produced contains a high density of regular stacking faults [7]. Although nominally fcc, these faulted structures are more generally described as orthorhombic or monoclinic, depending on how they are indexed.

However, shear on a single $\{110\}<1\bar{1}0>$-type system cannot readily account for the formation of a *tetragonal* martensite. This deficiency is remedied in the well-known phenomenological theory of martensite crystallography (PTMC) which can account for a tetragonal martensite using a combination of lattice deformation and macroscopic shape deformation. However, in yet another approach to the same problem, an approximately tetragonal martensite can also be obtained from two shears, as in the double shear mechanism of Bowles, Barret and Guttman, proposed 1950 [8]. In this mechanism, shear took place sequentially along two $\{110\}<1\bar{1}0>$ systems, *eg*. first along $(101)[10\bar{1}]$ to produce a monoclinic structure and then along $(110)[1\bar{1}0]$ to produce a triclinic crystal that it is very nearly tetragonal. Extending this principle, a perfectly tetragonal martensite, in this case with $c/a<1$, can be conceptually produced from a cubic parent by the simultaneous application of four independent $\{110\}<1\bar{1}0>$-type shears, provided that the principle of linear superposition can be applied. (In terms of this principle, which is valid for Hookean elastic solids, the waves, shear or otherwise, can travel through the solid quite independently of one another). The superposition of the shears will produce, by vector addition, a net displacement of atomic co-ordinates that gives the product structure, without the need to invoke an irrational shear system (Figure 1). If all four shear systems operate simultaneously, and if the value of the shear strain (ε) of each is equal, then the vector sum of all the displacement components is as given in Table 1. It is evident that the δz displacement is of opposite sign and twice the magnitude of the δx or δy displacements. Once divided in each case by the starting cubic lattice parameter, these become the lattice dilation/contraction strains, ε_x, ε_y, and $\varepsilon_z=-2\varepsilon_x$, a condition which

has been shown [9] to produce a habit plane between parent and martensite that is close to {011} and a minimal change in the volume of the unit cell.

Application of a ε_x of 2% to the cubic parent phase of $Au_7Cu_5Al_4$, which has a unit cell of a_o=0.616 nm, will produce a martensite unit cell with a=b=0.628 nm, c=0.591 nm. Further adjustment to the measured values [4] of a=b=0.630 nm, c=0.594 nm in the actual crystal (corresponding to ε_x= 2.27% and ε_z= -3.57%) could conceivably take place in the lattice by thermally-induced relaxation, or the deviation could be the result of some additional faulting or modulation in the structure.

It is recognised that the PTMC and the 'two-' and 'four-shear' mechanisms are not completely compatible. In particular, the latter do not require, in principle, an interface between parent and product phases, whereas the reaility is that the transformation takes place by means of the movement of a well-defined interface between parent and product. Furthermore, there is the complication of retaining a common plane (the 'habit plane') between parent and product phases during the transformation. If the four-shear mechanism operates at all, it can only be in the immediate vicinity of the habit plane. However, one advantage of the 'four-shear' explanation is that it invokes the known lattive vibration modes to explain the atomic displacements, whereas the PTMC is silent on this issue.

Irrespective of its mechanism of formation, the normal, **n**, to the habit plane of the tetragonal martensite can be calculated from the values of ε_x and ε_z, using the formula [9]

$$\mathbf{n} = \left[0, \sqrt{\left(\frac{|\varepsilon_{33} + \varepsilon_{11}|}{|\varepsilon_{11}| + |\varepsilon_{33} + \varepsilon_{11}|} \right)}, \sqrt{\left(\frac{|\varepsilon_{11}|}{|\varepsilon_{11}| + |\varepsilon_{33} + \varepsilon_{11}|} \right)} \right] \qquad (1)$$

where ε_{11}=ε_x and ε_{33}=ε_z. The result for the nominal values of ε_x=2.0% and ε_z=4.0% is the expected (0 1 1) habit plane. However, substitution of the measured values of ε_x and ε_z for this transformation

give a normal vector with co-ordinates (0, 0.600, 0.797). This corresponds to a (0 3 4) habit plane, the normal of which makes an angle of close to 8° to the normal to the (0 1 1) habit plane.

The X-ray diffraction spectrum calculated for a perfectly tetragonal martensite is compared in Figure 2 to some measured examples for this martensite. In general, there are small extra peaks on the experimental martensite spectra. There were, in general, four prominent sets of extra peaks, denoted 'a' to 'd' on the Figure. It has been shown previously that these extra peaks may be reproduced if the tetragonal symmetry of the martensite is reduced by either modifying the lattice occupancies or by arbitrarily displacing certain of the atoms from their nominal positions [4]. However, the measured martensite spectra were produced with a phase transformation that exhibited strong first-order characteristics [3]. Therefore, a change in occupancy of the lattice sites during the transformation can be eliminated, leaving positional modulation of the atoms as the probable cause.

3.2 The case for modulation

Modulation by a single shear wave

The $<0\bar{1}1><011>$ phonon soft mode mentioned previously is often prominent in B2 structures as the temperature of transformation to martensite is approached from above. However, it is important to note that other lattice instabilities or combinations of lattice instabilities can operate prior to or during a martensite transformation. Also, the soft mode phenomenon is not necessarily directly correlated with martensitic transformation, and the presence of a vibrational soft mode does not guarantee that a martensitic transformation will take place [5], nor are all martensitic transformations necessarily driven by solely by soft mode phenomena [10]. Nevertheless, much of the atomic movement necessary to produce, for example, a B19 martensite from a B2 parent, is very neatly explained as being the result of the application of a $[11\ 0]_\beta/[\bar{1}\,10]_\beta$ shear wave (the first term refers to the direction of propagation **k** and the second to the polarization **e** of the transverse displacement wave) with a

wavelength of $\sqrt{2}a_\beta$, where a_β is the unit cell dimension of the parent B2 phase [11] (Figure 3). Of course, some homogenous dilation and/or contraction of the lattice may also be required. The concept of a soft mode shear wave therefore has some utility, at least in a pedagogic context, in explaining the formation of hexagonal martensites from bcc parents.

The net effect of the application of the hypothetical shear wave is that the new atomic positions are related to the old in two of the three lattice directions by a sinusoidal mathematical expression. In the case of the B19 structure of AuCd, for example, it can be seen from Figure 3 that

$$\Delta k = A.\sin(2\pi i) \qquad (2)$$

where i is the fractional distance (varying from 0 to 1) along the B2 z-face diagonal (eventually the a_{B19}-axis) of the atom to be modulated, and Δk is the displacement from the nominal position in the c_{B19}-direction. The resulting crystal structure can therefore justly be considered to be a 'modulated' derivative of the original cubic parent structure, that is, its atomic positions are displaced from the nominal starting lattice positions by some periodic oscillation.

If the parent has B2 ordering, then the modulated and parent structures can be shown to be both members of the set of diverse close-packed B19 crystal structures. This follows because the basis vectors of the generic B19 crystal structure are [12]

$$\mathbf{B}_1 = \tfrac{1}{4}a\mathbf{X} + x_1 c\mathbf{Z}$$

$$\mathbf{B}_2 = -\tfrac{1}{4}a\mathbf{X} - x_1 c\mathbf{Z}$$

$$\mathbf{B}_3 = \tfrac{1}{4}a\mathbf{X} + \tfrac{1}{2}b\mathbf{Y} + x_2 c\mathbf{Z}$$

$$\mathbf{B}_4 = -\tfrac{1}{4}a\mathbf{X} - \tfrac{1}{2}b\mathbf{Y} - x_2 c\mathbf{Z} \qquad (3)$$

where **X**, **Y** and **Z** are the principle axes, *a*, *b* and *c* are the B19 lattice parameters and x_1 and x_2 are parameters that control the modulation of the atoms. Vectors $\mathbf{B}_1$ and $\mathbf{B}_2$ apply to the first element (*eg*. Cd) and $\mathbf{B}_3$ and $\mathbf{B}_4$ to the second (eg. Au). Substitution of unit axes into the expressions generates the atomic positions of the four atoms in the conventional representation of the B19 unit cell.

The usefulness of this generic structure can be seen by noting that, if $a=b=c$, $x_1=0.25$, $x_2=x_1+0.5$, and there is only one kind of element, then the structure is A1 (fcc). If $a=c$, $x_1=0.25$, and $x_2=x_1+0.5$, then the structure is $L1_0$. If $\frac{a}{b}=\left(\frac{8}{3}\right)^{2/3}$, $\frac{c}{b}=(3)^{1/2}$, $x_1=5/6$ and $x_2=1/3$ and there is only one kind of element then the structure is hexagonal close packed [12]. If $a=c$ and $\frac{a}{b}=\sqrt{2}$ then the structure is B2, or if there is only one kind of element, A2. Finally, it can be shown that the strongly modulated B19 structure of AuCd, for example, may be obtained from a B2 parent, by allowing a≠c, $\frac{a}{b}\neq\sqrt{2}$ and increasing x_1 to 0.31 [12].

Higher order modulation

In general, it seems that the structures of many martensites are modulated to a greater or lesser extent. However, this modulation will rarely be as simple or complete as in the case of the B19 AuCd given above. It has been claimed in some instances that this modulation is directly related to the soft mode lattice instability that was associated with their formation [11,13]. In a widely used scheme, various martensite structures are differentiated in terms of the number of basal planes corresponding to the wavelength of the modulation or repetition. For example, the martensite formed from $Ni_{0.64}Al_{0.36}$ may be denoted 7M (or 14M according to a different notation [14]) and it is formed by a modulation along the [110] cubic direction with an effective wavelength of seven times the basal plane spacing [15]. Other structures with five, twelve or fifteen layers of basal planes have also been reported [14].

Of particular interest is that some investigators of the other tetragonal martensites have linked 'extra' X-ray diffraction peaks, such as those shown in Figure 2, to such positional modulations in the lattice. Webster *et al.* [16], for example, who found such extra peaks in spectrum of the low temperature form of Ni_2MnGa, speculated that they were due to periodic stacking faults, lying perpendicular to the c-axis direction of the bct lattice, and with a modulation of 'at least four planes'. This point has been investigated in more detail by later workers, who have elucidated the nature of these modulations in this compound in some detail [14,17]. However, as mentioned, some of the 'extra' peaks can potentially be generated by making non-symmetrical changes to lattice site occupancies. The present authors also found that the introduction of regularly spaced anti-phase domain boundaries could result in the generation of these and other extra peaks. However, since no independent evidence of such site occupancy change or chemical modulation is so far known for this system, these lines of inquiry are not pursued further here, and it is considered more likely that in this case the atomic *positions* of the present $Au_7Cu_5Al_4$ martensite were modulated, and that this might explain some or all of the 'extra' diffraction peaks.

The $<0\bar{1}1><011>$ displacement in Ni_2MnGa produces a 'roughly' tetragonal martensite with 5M modulation (10M according to the notation used by Pons *et al.* [14]) parallel to the basal $(001)_M$ plane or former $(110)_\beta$ plane [15,17]. It is actually a two step process with a 3M modulated martensite in-between [15]. It appears that accurate description of the modulation may require more than just a single sinusoidal waveform, and for example in the case of Ni_2MnGa the displacement of the successive $(110)_\beta$ planes (or (220) planes if they are indexed on the same 16 atom unit cell as the parent Heusler phase) can be described by a three-term sinusoidal expansion [17]:

$$\Delta l = A.\sin\left(\frac{2\pi l}{5}\right) + B.\sin\left(\frac{4\pi l}{5}\right) + C.\sin\left(\frac{6\pi l}{5}\right) \qquad (4)$$

where Δl is the displacement in the direction of the wave's polarization of the atom at distance l along the direction of the wave's propagation. A, B and C are coefficients to be determined by analysis of the experimental data. Obviously if the modulation is not 5M then a different denominator is required in the expression.

Another important point is that these soft mode-driven (or, perhaps, merely associated) transformations need not be completely 1st order in nature. Shapiro [15] has pointed out that the soft mode phenomenon can explain the 2nd order characteristics of many displacive transformations too. The soft mode or shear wave is coincident with the atomic displacement necessary to form the low temperature phase. The product phase forms when the vibration 'freezes'. This may be the origin of the observation that martensitic transformations in Hume Rothery compounds are 'weakly 1st order' [*eg*. 5, 11].

It is interesting that the 'classic' and rigorous application of the soft mode instability mechanism for martensite formation from a cubic parent phase, which would require that the $(c_{11}-c_{12})/2$ shear modulus should reduce to a magnitude of zero at the M_s temperature, is said to be always correlated with a tetragonal transformation product [18]. If this observation is genuinely universal, then it implies that the present $Au_7Cu_5Al_4$ parent phase should also be susceptible to the phenomenon of complete softening, unlike the case for nearly all other non-ferrous systems, such as Ni_xAl_{1-x} or other noble metal Hume-Rothery compounds, in which only a relative reduction in $(c_{11}-c_{12})/2$ occurs prior to transformation. However, there is reportedly not complete softening in Ni_2MnGa eg. [15], this exception presumably disproving the rule.

4. Modulation of the $Au_7Cu_5Al_4$ martensite lattice

4.1 Determination of the modulation wavelength

To begin with, as with previous workers who investigated Ni_2MnGa [16,17], the modulation was investigated using the tetragonal version of the 16 atom $L2_1$ unit cell of the parent phase. For this unit cell, a single sinusoidal modulation in the *a-b* (*x-y*) plane with a wavelength of three {220} planes (Figure 4) may be described by the generalised parametric equations

$$x' = x + \varepsilon_1 . \cos(4\pi j) . \cos(45°)$$

$$y' = y - \varepsilon_1 . \cos(4\pi j) . \sin(45°), \text{ and}$$

$$z' = z \qquad (5)$$

where *x*, *y* and *z* are the nominal positions on the tetragonal lattice, *x*′, *y*′ and *z*′ are the positions after the application of the modulation waves, ε_1 is the amplitude of the modulation wave, and *j* is the fractional distance across the *a-b* plane of the 16 atom unit cell in the [110] direction.

After allowing for modulations of other numbers of {220} planes, such as the 5M modulation reported for Ni_2MnGa and NiAl, the parametric equations become (after simplification):

$$x' = x + \frac{\varepsilon_1}{\sqrt{2}} \cos\left(\frac{8\pi j}{M-1}\right)$$

$$y' = y - \frac{\varepsilon_1}{\sqrt{2}} \cos\left(\frac{8\pi j}{M-1}\right), \text{ and}$$

$$z' = z \qquad (6)$$

where *M* is the order of the modulation (3 for 3M modulation and 5 for 5M modulation, respectively equivalent to the 6M and 10M modulation of some other workers [14]).

Diffraction spectra were calculated for the present martensite using a 64 atom unit cell consisting of 4 16 atom *tI*16 unit cells in 2x2x1 configuration. For reasons of symmetry, this allowed only 3M, 5M and 9M modulations to be tested, since the wavelength of the modulation had to divide into the *z*-face diagonal of the unit cell by an integer factor, and also for it to be some integer multiple of the wavelength of $L2_1$ atomic ordering in that direction. It was observed that the introduction of the modulations enabled all the observed extra peaks to be explained, but undesired, extra peaks were simultaneously introduced. In particular, the 3M modulations reproduced the peaks at positions *b*, *c* and *d* in Figure 3, and the 5M modulation reproduced the peak at 0.237 nm (position *e* on Figure 4). However, the 9M modulation scheme consistently produced a peak at 0.250 nm (position *f* on Figure 4), which was never observed on any experimental spectrum. The 5M scheme, however, had the deficiency of not producing peaks *c* and *d*, and not one of these three schemes produced a peak at position *a*. On balance, it was concluded that the 3M modulation system most generally simulated the measured spectra. However, it was clear that a few samples possessed spectra with features like those calculated for 5M modulation. These samples had in common the fact that they contained only between 4 and 5 wt.% Al (compared to the usual 5.8 wt% Al of most other samples). Further work is needed to verify this tentative correlation.

It should be noted that a simple one-term sinusoidal transverse wave may in practice be something of an over-simplification, and in some cases investigators invoked higher harmonics of the basic wave [17]. Similarly, there are other modulation wavelengths (*eg.* 4M, 6M, 7M *etc*) which the present authors have not yet attempted. Therefore, the possibility that the spectra can be better explained as being the outcome of something more complex than a $<0\bar{1}1><011>$ shear wave with 3M or 5M modulation wavelengths remains unexplored. Nevertheless, since the 3M scheme was able to account for much of the observed detail in the diffraction spectra, it was selected for the next part of the exercise, which was to determine the modulation amplitude.

4.2 Determination of the 3M (B19) modulation amplitude

It was shown earlier that the most general form of the B19 close-packed lattice requires five parameters for description of atomic positions. The parameters are *a*, *b* and *c* (the B19 lattice parameters), and x_1 and x_2, which control the displacement of the atoms off the unmodulated lattice positions. However, the present martensite is formed from an $L2_1$ parent rather than from a B2 one, so a full description of it requires a doubling of the B19 unit cell in the *b* direction, in order to account for the additional, ternary, atomic ordering. Furthermore, as a simplification, we have set $x_2=x_1+0.5$, a situation required by the geometry of the B19 unit cell [19]. The resulting atomic positions are listed in Table 2, and the generic unit cell is illustrated in Figure 5. The site occupancies are presumed to be the same as those previously estimated for the parent phase [2]

The *a*, *b* and *c* parameters of the new unit cell may be calculated from those of the 16 atom $L2_1$-derived one by using the geometric relationships shown in Figure 3, which would give $a=c=0.4455$ nm, and $b=0.594$ nm. However, for greater accuracy, the analysis of the experimental XRD spectra was repeated, this time in orthorhombic space, to produce $a=0.4465$ nm, $b=0.594$ nm and $c=0.4435$ nm. The lattice positions and occupancy data shown in Table 2 were then combined with these dimensions, and x_1 systematically varied to find the value of it that best fitted the observed average heights of peaks b, c and d. The results (Figure 6) indicated that the difference between the measured and calculated intensities of the peaks b, c and d is minimised at values of x_1 that are respectively 0.288, 0.290 and 0.301. Of course, these values should be the same, illustrating the limitations of our present experimental measurements. However, it can be stated that the value of x_1 that best reproduces the experimental spectra is 0.293 ± 0.05, which is sufficient to show that the martensite is modulated somewhat less than B19-AuCd.

5. Adaptive twinning

It has been shown above that the martensite is not perfectly tetragonal, and that it is both modulated and very slightly orthorhombic. Nevertheless, from a geometric perspective, it is nominally tetragonal, sufficiently so, we believe, to allow the application of the existing literature on cubic-to-tetragonal transformations. For example, it has been shown that wedge-shaped laths occur in the present system, a point believed to be uniquely diagnostic of cubic-to-tetragonal martensites [4,20].

The displacive transformation from a cubic to a tetragonal phase (and vice versa on heating), or from one tetragonal variant to another, generates considerable strain in a macroscopic sample. However, opposing this, there is also a requirement in these systems that the parent and product phases have a coherent relationship across their mutual interfaces. The mismatch in lattice spacing between cubic and tetragonal phases is reduced by them sharing a habit plane, which is common to both lattices, and in some cases, by adaptive twinning or microtwinning of the martensite. The principles upon which the microtwinning in tetragonal structured martensites are based have been elegantly stated by Khachaturyan *et al.* [9]. They have shown how coherency can be achieved if the martensite forms twins at the scale of a few lattice planes per twin variant. At this scale the twins are almost like stacking faults or shuffles. These 'adaptive martensites' are likely to form if the surface energy of twin boundaries is relatively low while the lattice mismatch between cubic parent and tetragonal product is relatively high. The B19 AuCd martensite is known to be microtwinned, illustrating that, while not strictly tetragonal, it too is susceptible to these same considerations.

In practice, adaptive martensite consists of a periodic alternation of two twin variants, of thickness d_1 and d_2 respectively. For these very fine-scale twins, $d_1=m.a_{tw}$ and $d_2=n.a_{tw}$, where m and n are integers, and a_{tw} is the interatomic spacing of the $\{110\}_{B2}$ twinning planes. Of particular interest here is that Khachaturyan *et al.* showed that there are special values of m and n that provide the minimum

interface misfit for a given combination of parent and product phase lattice parameters. If the volume fraction of the variant with thickness d_1 is ω, then it follows that

$$\frac{d_1}{d_2} = \frac{m}{n} = \frac{\omega}{1-\omega} \tag{7}$$

For invariant plane strain

$$\omega = \frac{\varepsilon_x}{\varepsilon_x - \varepsilon_z} > 0 \tag{8}$$

where $\varepsilon_x=\varepsilon_y$, and these lattice strains are as defined earlier.

In the case of the present system, ε_x=+2.27% and ε_z=-3.57%, thereby indicating an ω of 0.389 for the variant with thickness d_1 or, quite equivalently, an ω of 0.611 for the other variant. A wide range of *m* and *n* values can in principle meet the requirements of Equations (7) and (8). However, not all values of *m* and *n* generate simple two-variant stacking sequences that correctly repeat at the second twin boundary. Those that do are listed in Table 3 for *m*>=*n*, and these form the super-set out which the selection must be made in the present exercise. The notation used for these martensites follows Khachaturyan *et al.* [9]. The stacking sequences of two examples of two-variant adaptive martensite, and one multiple variant adaptive martensite are shown in Figure 7, together with the corresponding notation, to illustrate the system. All crystallographically valid structures must begin and end on the same type of stacking fault, which, for example, makes some stacking schemes, such as $5R(3,\bar{2})$, impossible in terms of this notation. The $5R(3,\bar{2})$ structure is however, simply a 5M modulated lattice which could perhaps be approximately represented by the notation $5R(2\frac{1}{2},\bar{2}\frac{1}{2})$. However, it is evident

that a valid two-variant 18R structure, for example, may form with the $(9,\bar{9})$, $(12,\bar{6})$ or $(15,\bar{3})$ stacking schemes.

This list of candidates may be culled by noting that TEM observations of this martensite have indicated that twins or 'lattice fringes' in the microstructure occur with an average individual width of between 7 and 10 $(110)_{cubic}$ planes [4], indicating that the adaptive structure (which would consist of pairs of twins) ought to have stacking height in the range 14R to 20R. From the 'ideal' volume fraction ω of 0.611 and Equation (7) it is evident that a ratio of m/n of about 1.5 to 1.6 would provide optimum coherency with the lattice of the parent phase. The structures thus pinpointed are listed in Table 4, in which it is also evident that a $15R(9,\bar{6})$ martensite appears to offer the closest match. However, this does not properly reproduce the inherited $L2_1$ ordering across its extremities, and should actually be doubled to make a 30R martensite with fourfold $(9,\bar{6},9,\bar{6})$ adaptive twinning, which does.

6. Conclusions

The martensite produced from the $L2_1$-ordered $Au_7Cu_5Al_4$ β electron compound parent phase may be described as a first approximation to be tetragonal, with $c/a \approx 0.94$. It shares behavioural attributes with other cubic-to-tetragonal martensites, such as Ni_xAl and Ni_2MnGa. These attributes include forming wedge-shaped laths and adaptive twins, and modulated structures. However, detailed analysis shows that the present structure is approximately sinusoidally modulated on the 3M scheme, and it is therefore more accurately described as B19, with the unit cell doubled to account for the $L2_1$ ordering inherited from the parent phase. The amplitude of the modulation parameter x_1 was estimated and found to be only about ~0.29 compared to the ~0.31 of Au-47 at.%Cd, a classic B19 martensite. Some evidence for 5M modulation in Al-lean compositions was found. In this respect the present martensite is probably akin to that in Ni_2MnGa, which shows a diversity of structures depending on stoichiometry

and thermal processing. Finally, the probable nature of the adaptive microtwinning was explored, and it appears that a $15R(9,\bar{6})$ stacking would provide optimum mimimisation of strain across the habit plane. However, this does not correctly propagate the inherited $L2_1$ order, so a doubling of this stacking scheme to $30R(9,\bar{6},9,\bar{6})$ is actually required for symmetrical reasons. It is very unlikely, however, that the martensite is perfectly stacked on this scheme, and it is therefore merely a convenient approximation of what is probably a less regular defect structure.

Acknowledgements

This paper is published by permission of Mintek.

References

[1] Wolff IM, Cortie MB. Gold Bull. 1994; 27(2):44.

[2] Cortie MB, Levey FC. Intermetallics 2000; 8:793.

[3] Levey FC, Cortie MB, Cornish LA. Metall. Materials Trans. A 2000; 31A:1917.

[4] Levey FC, Cortie MB. Mater. Sci. Eng. A 2001; A303:1.

[5] Wasserman EF, Kästner J, Acet M, Entel P. In: Koiwa M et al, editor. Proc. Int. Conf. on Solid-Solid Phase Transformations '99, (JIMIC-3). Sendai, Japan : The Japan Institute of Metals, 1999. p.807.

[6] Zener C. Phys. Rev. 1947; 71(12):846.

[7] Warlimont H, Delaey L. Progr. Mater. Sci. 1974; 18:1.

[8] Bowles JS, Barrett CS, Guttman L. J. Met., Trans. AIME 1950; 188:1478.

[9] Khachaturyan AG, Shapiro SM, Semenovskaya S. Phys. Rev. B 1991; 43(13): 10832.

[10] Krumhansl JA. J. de Physique IV, Colloque C2, supplement to J. de Physique III 1995; 5:3.

[11] Barsch GR, Ohba T, Hatch DM. Mater. Sci. Eng. A 1999; A273-275:161.

[12] Mehl, MJ. Naval Research Laboratory, USA, Internet site, http://cst-www.nrl.navy.mil /lattice /struk/b19.html, accessed November 2000.

[13] Zheludev A, Shapiro SM, Wochner P, Schwartz A, Wall M, Tanner LE. J. de Physique IV, Colloque C8 1995; 5: 1139.

[14] Pons J, Chernenko VA, Santamarta R, Cesari E. Acta Mater. 2000; 48:3027.

[15] Shapiro SM. In: Koiwa M et al, editor. Proc. Int. Conf. on Solid-Solid Phase Transformations '99, (JIMIC-3). Sendai, Japan : The Japan Institute of Metals, 1999. p.799.

[16] Webster PJ, Ziebeck KRA, Town SL, Peak MS. Philos. Mag. B, 1984; 49(3): 295.

[17] Martynov VV. J. de Physique IV, Colloque C8, supplement to J. de Physique III, 1995; 5:91.

[18] Khachaturyan AG. Theory of Structural Transformations in Solids, Wiley-Interscience, New York, 1983.

[19] Dwight AE, Conner RA, Downey JW. Acta Cryst. 1965; 18:837.

[20] James RD, Hane KF. Acta Mater. 2000; 48:197.

FIGURE CAPTIONS

Figure 1. The four shear systems, which if applied simultaneously, will give a cubic-to-tetragonal phase transformation. The numbering system used in Table 1 is shown bottom right.

Figure 2. Calculated X-ray spectrum of tetragonal martensite and examples of actual measured martensite spectra.

Figure 3. Formation of B19 martensite from B2 parent by application of a [101]/[$10\bar{1}$] shear wave, a. top view, b, rotated view. The atomic displacements that transform the B2 lattice into the B19 lattice are omitted from the rotated view for clarity.

Figure 4. Calculated X-ray diffraction spectra for various modulation schemes. 3M spectrum computed for ε_1=0.015 nm, 5M spectrum for ε_1=0.022 nm and 9M spectrum for ε_1=0.030 nm. Peaks at positions *b*, *c*, *d* and *e* may be found on selected experimental spectra.

Figure 5. Doubly-extended B19 unit cell, as applied to the present martensite

Figure 6. Error in height of peaks *b*, *c* and *d* on spectra calculated for various 3M modulation amplitudes, with respect to average peak height on five experimental spectra.

Figure 7. Stacking sequences of common 9R martensite, and those of hypothetical $5R(4,\bar{1})$ and $8R(4,\bar{4})$ martensites, given here to illustrate the notation used. Dashed lines indicate the position of notional stacking faults.

TABLES

Table 1. Atomic displacements δx, δy and δz produced by four independent shear actions on atoms 1 to 4 in Figure 1, and their vector addition. (The displacements of the unnumbered atoms lying on the lower face may be shown to be simply the reflection across the (002) plane of those on the upper face.)

	Atom 1	Atom 2	Atom 3	Atom 4
$(101)[10\bar{1}]$	0, 0, 0	δx, 0, $-\delta z$	$+\delta x$, 0, $-\delta z$	0, 0, 0
$(01\bar{1})[011]$	0, $-\delta y$, $-\delta z$	0, $-\delta y$, $-\delta z$	0, 0, 0	0, 0, 0
$(10\bar{1})[101]$	$-\delta x$, 0, $-\delta z$	0, 0, 0	0, 0, 0	$-\delta x$, 0, $-\delta z$
$(011)[01\bar{1}]$	0, 0, 0	0, 0, 0	0, δy, $-\delta z$	0, δy, $-\delta z$
Vector sum	$-\delta x$, $-\delta y$, $-2\delta z$	$+\delta x$, $-\delta y$, $-2\delta z$	$+\delta x$, $+\delta y$, $-2\delta z$	$-\delta x$, $+\delta y$, $-2\delta z$

Table 2. Cartesian positions and lattice occupancies of sites in the 3M unit cell of the present martensite, derived by doubling of a generic B19 unit cell.

Site	Nature	x	y	z	Occupancy		
					Au	Cu	Al
1	Au-rich	¼a	0	x_1c	0.653	0.328	0.019
2	Au-rich	-¼a	0	$-x_1c$	0.653	0.328	0.019
3	Al-rich	¼a	¼b	x_2c	0.168	0.244	0.588
4	Cu-rich	-¼a	¼b	$-x_2c$	0.267	0.388	0.345
5	Au-rich	¼a	½b	x_1c	0.653	0.328	0.019
6	Au-rich	-¼a	½b	$-x_1c$	0.653	0.328	0.019
7	Cu-rich	¼a	¾b	x_2c	0.267	0.388	0.345
8	Al-rich	-¼a	¾b	$-x_2c$	0.168	0.244	0.588

Table 3. Valid two-variant microtwinned adaptive martensites formed from a disordered cubic parent. Only entries for $m>=n$ are given, the entries for $n<m$ may be derived by reflection.

m	n											
	1	2	3	4	5	6	7	8	9	10	11	12
1	2R											
2		4R										
3			6R									
4	5R			8R								
5		7R			10R							
6			9R			12R						
7	8R			11R			14R					
8		10R			13R			16R				
9			12R			15R			18R			
10	11R			14R			17R			20R		
11		13R			16R			19R			22R	
12			15R			18R			21R			24R
13	14R			17R			20R			23R		
14		16R			19R			22R			25R	
15			18R			21R			24R			27R
16	17R			20R			23R			26R		
17		19R			22R			25R			28R	

Table 4. Short-list of martensite structures with approximately correct twin width and lattice misfit strain.

Structure	m/n
$15R(9,\bar{6})$	1.50
$17R(10,\bar{7})$	1.43
$19R(11,\bar{8})$	1.38
$20R(13,\bar{7})$	1.86

FIGURES

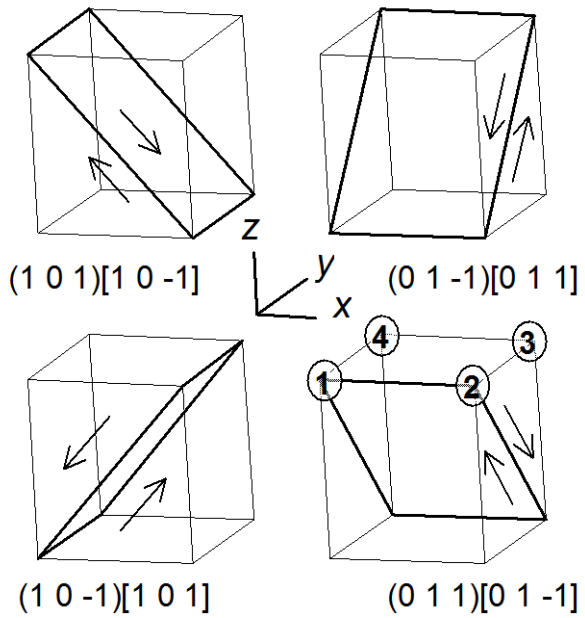

Figure 1. The four shear systems, which if applied simultaneously, will give a cubic-to-tetragonal phase transformation. The numbering system used in Table 1 is shown bottom right.

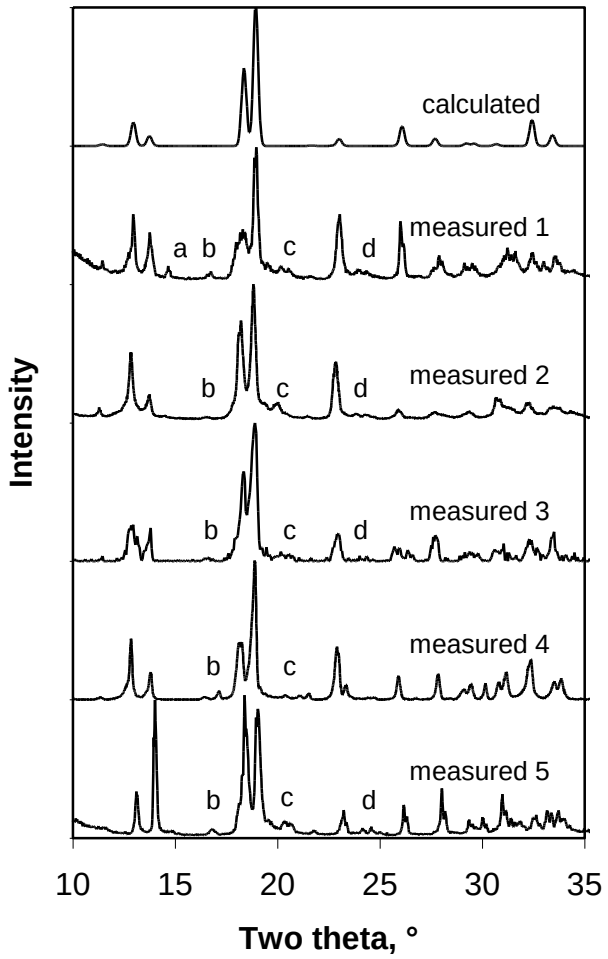

Figure 2. Calculated X-ray spectrum of tetragonal martensite and examples of actual measured martensite spectra.

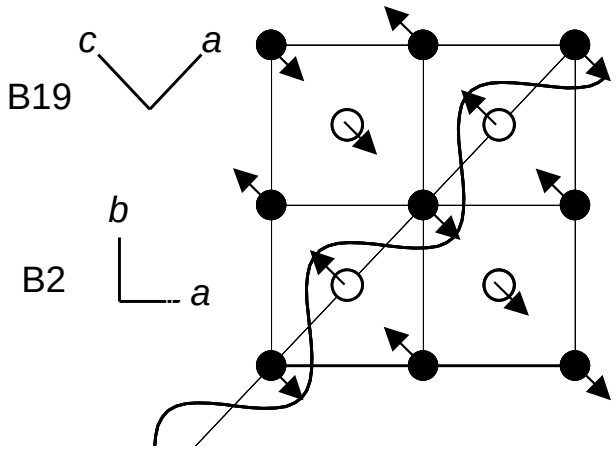

a

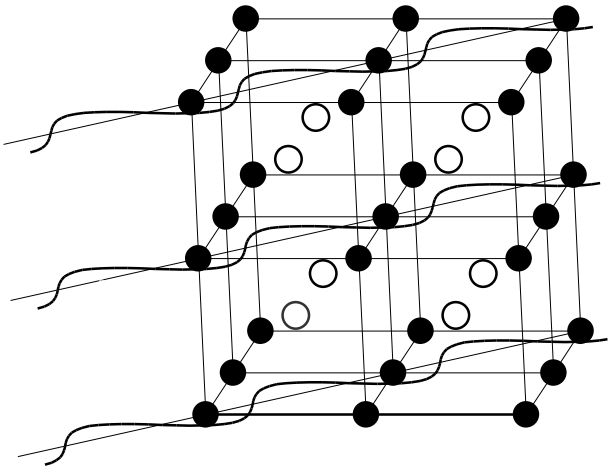

b

Figure 3. Formation of B19 martensite from B2 parent by application of a [101]/[$1\bar{0}1$] shear wave, a. top view, b, rotated view. The atomic displacements that transform the B2 lattice into the B19 lattice are omitted from the rotated view for clarity.

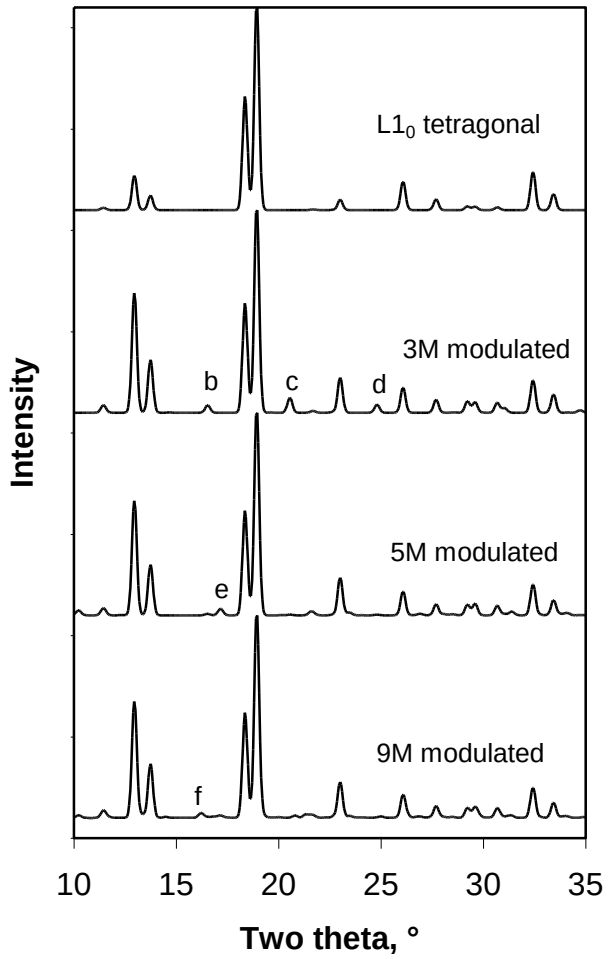

Figure 4. Calculated X-ray diffraction spectra for various modulation schemes. 3M spectrum computed for ε_1=0.015 nm, 5M spectrum for ε_1=0.022 nm and 9M spectrum for ε_1=0.030 nm. Peaks at positions *b*, *c*, *d* and *e* may be found on selected experimental spectra.

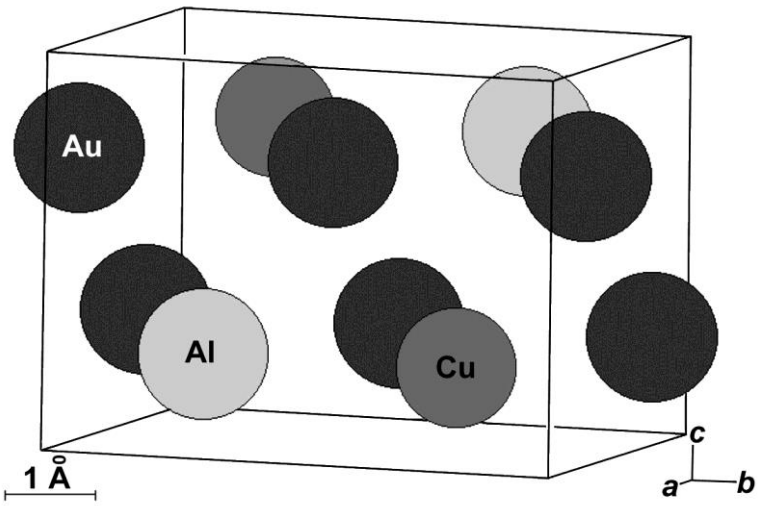

Figure 5. Doubly-extended B19 unit cell, as applied to the present martensite

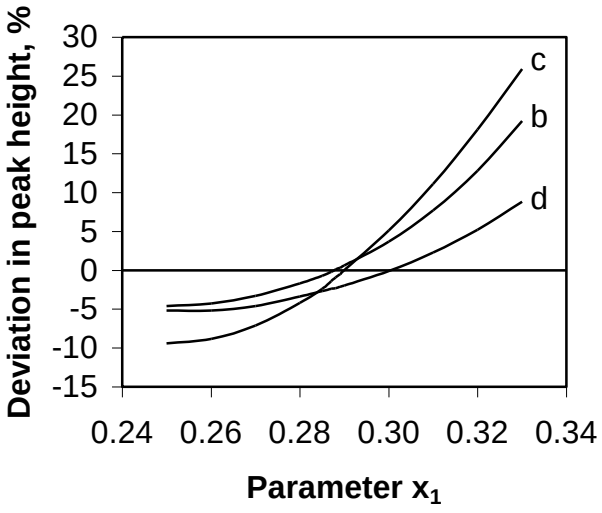

Figure 6. Error in height of peaks *b*, *c* and *d* on spectra calculated for various 3M modulation amplitudes, with respect to average peak height on five experimental spectra.

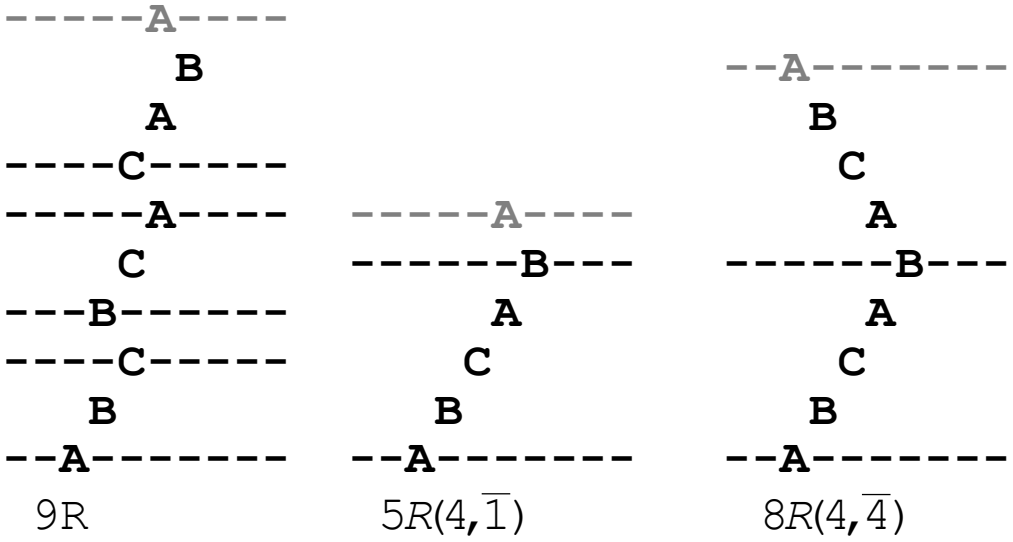

Figure 7. Stacking sequences of common 9R martensite, and those of hypothetical $5R(4,\bar{1})$ and $8R(4,\bar{4})$ martensites, given here to illustrate the notation used. Dashed lines indicate the position of notional stacking faults.